J Soils Sediments (2018) 18:1641–1653
https://doi.org/10.1007/s11368-017-1866-2

SOILS, SEC 5 • SOIL AND LANDSCAPE ECOLOGY • RESEARCH ARTICLE

Surface liming effects on soil radiation attenuation properties

Talita R. Ferreira[1] · **Luiz F. Pires**[2] · **André M. Brinatti**[2] · **André C. Auler**[3]

Received: 2 March 2017 / Accepted: 3 November 2017 / Published online: 13 November 2017

Abstract
Purpose This study investigates the effects of surface liming on soil attenuation radiation properties. For this, measurements of soil chemical attributes (pH, organic carbon, H+Al, Al^{3+}, Ca^{2+}, and Mg^{2+}) and attenuation radiation parameters (mass attenuation coefficient, μ_m, atomic and electronic cross sections, σ_a and σ_e, effective atomic number and electron density, Z_{eff} and N_{el}) were carried out. This aim was motivated by the fact that possible μ_m variation might cause as well variation in the determination of soil physical properties.
Materials and methods The studied soil, classified as a Dystrudept sity-clay, is located in South Brazil. The trial consisted of five stripes, one of them under pasture and the remaining under no-till system (NTS). Lime rates of 0, 10, 15, and 20 t ha^{-1} were broadcast on the NTS soil surface. Disturbed soil samples were collected 30 months after liming at the top (0–10 cm) and subsoil (10–20 cm) layers. Soil chemical attributes were characterized following standard experimental procedures. The soil oxide composition, obtained by EDXRF analysis, was used to calculate μ_m for ^{241}Am and ^{137}Cs photon energies with XCOM computer code. μ_m values were employed to calculate σ_a, σ_e, Z_{eff}, and N_{el} and to predict variations in soil bulk density (ρ) and total porosity (φ).
Results and discussion Surface liming notably increased contents of soil pH, Ca^{2+}, and Mg^{2+} while reduced H+Al and Al^{3+} at the top soil layer, where μ_m, σ_a, σ_e, and Z_{eff} were also increased with the lime rates. However, at the subsoil layer, liming neither lessened soil acidity nor induced remarkable changes in the attenuation parameters. When using ^{137}Cs photon energy, incoherent scattering totally dominated over the radiation interaction processes whereas photoelectric absorption and coherent scattering substantially contributed when ^{241}Am photon energy was used. Therefore, the increasing in soil attenuation parameters at the top soil layer was more accentuated considering ^{241}Am than ^{137}Cs photon energy. Variation in μ_m caused considerable variation in ρ and φ only for ^{241}Am photon energy.
Conclusions The findings regarding the effect of μ_m variation induced by liming on the determination of soil physical properties are extremely relevant because traditionally, in the soil science area, μ_m values are calculated without considering any chemical modification to which the soil can be submitted. Bearing in mind that ρ and φ are important parameters from the agricultural and environmental points of view, not representative measurements of μ_m can lead to biased values of ρ and φ.

Keywords Liming · Mass attenuation coefficient · Soil acidity · Soil attenuation properties · XCOM · X-ray fluorescence

Responsible editor: Arnaud Temme

✉ Talita R. Ferreira
tali.rf@gmail.com

[1] Physics Graduate Program, Department of Physics, State University of Ponta Grossa (UEPG), Ponta Grossa, Brazil

[2] Laboratory of Physics Applied to Soil and Environmental Sciences, Department of Physics, State University of Ponta Grossa (UEPG), Ponta Grossa, Brazil

[3] Agronomy Graduate Program, Department of Soil Science and Agricultural Engeneering, State University of Ponta Grossa (UEPG), Ponta Grossa, Brazil

1 Introduction

The mass attenuation coefficient (μ_m) is an important parameter for characterizing the penetration and diffusion of gamma radiation in multi-element materials (Hubbell 1969). This parameter can be determined experimentally by nuclear

techniques or theoretically by the knowledge of the soil chemical composition, with good agreement between these methodologies (Pires and Pereira 2014). The theoretical computation of μ_m for elements, compounds, or mixtures, in a wide energy range (1 keV to 100 GeV), can be easily accomplished with the help of computer codes specifically developed for this purpose, such as XCOM (Berger and Hubbell 1987) and its successor WinXCom (Gerward et al. 2004).

The aforementioned software programs take into consideration the absorption and scattering mechanisms (photoelectric absorption, Compton, pair production, and Rayleigh effects) by which the radiation is attenuated by the matter (Kaplan 1977). In the case of composite materials, the processes of radiation interaction are related to the effective atomic number and electron density (Z_{eff} and N_{el}), which are in turn dependent on the molecular, atomic, and electronic cross sections (σ_m, σ_a, σ_e) (Han and Demir 2009). All of these attenuation parameters can be predicted based on μ_m and the soil chemical composition, as reported in Medhat (2011) and Un and Sahin (2012).

A great number of studies regarding measurements of soil parameters such as water retention curve, water content, bulk density, and porosity have been performed by adopting attenuation of photons as an accurate, convenient, and non-destructive technique (Pires et al. 2005; Demir et al. 2008; Pires et al. 2009; Costa et al. 2013). However, it is important that any measurements of soil physical properties are representative of this porous media. Hence, when it comes to addition of soil amendments, such as lime, even though the variation in μ_m is likely to be slight, biased results may be obtained if such variation is not considered.

Liming is the most agriculture-employed practice to correct soil acidity. The use of Ca amendments such as limestone has been proven to increase soil pH and decrease exchangeable Al, increasing crop yield as a result (Mora et al. 1999). In addition, lime applications are particularly known to increase soil organic matter content in the long term (Haynes and Naidu 1998).

Besides changing the soil acidity, liming is also likely to promote variation of soil elemental composition. Dolomite limestone, for instance, generally contains 30.4% CaO, 21.8% MgO, and 47.8% CO_3 (Jones 2003). Thus, after solubilization, there might remain increased contents of CaO and MgO due to the non-reacted part of lime products. Here, these changes in the soil elemental composition can lead to modifications in μ_m.

The current research aims to investigate the effects of surface liming, 30 months past the lime application, on soil chemical attributes and soil attenuation properties, at the top and subsoil layers. This study also evaluates how possible differences in mass attenuation coefficients would promote changes in the soil bulk density and total porosity, considering the most common radioactive sources employed in soil physics (^{241}Am and ^{137}Cs).

2 Materials and methods

2.1 Soil sampling

The soil samples come from an experiment installed in May 2012, in a familiar rural site located in the Southeast region of Paraná State, Brazil (25°28′S, 50°54′W and 821 m a.s.l). The soil was classified as a Dystrudept silty-clay (Soil Survey Staff 2013).

The experimental area was designed in five stripes, one of them under pasture, considered as reference (Ref.), and the

Table 1 Chemical attributes for 0–10 cm (A) and 10–20 cm (B) soil layers (n = 4)

	pH	OC (g kg^{-1})	H + Al (cmol$_c$ dm^{-3})	Al^{3+}	Ca^{2+}	Mg^{2+}
Layer A						
Ref.	4.22 (0.22)	31.75 (6.29)	13.18 (2.72)	3.43 (2.04)	2.05 (1.09)	1.89 (0.76)
C0	3.93 (0.11)	36.50 (2.65)	15.35 (1.41)	4.15 (1.09)	1.53 (0.85)	2.55 (1.44)
C10	5.13 (0.43)	40.25 (7.59)	5.97 (2.04)	0.13 (0.15)	7.50 (2.16)	3.69 (2.45)
C15	5.59 (0.72)	42.00 (6.16)	4.31 (2.06)	0.10 (0.14)	8.95 (2.63)	4.63 (1.32)
C20	5.49 (0.48)	35.00 (1.83)	4.96 (2.11)	0.08 (0.05)	7.97 (1.75)	5.58 (0.88)
Layer B						
Ref.	3.95 (0.09)	18.50 (3.11)	16.82 (0.94)	6.30 (0.83)	0.90 (0.41)	1.01 (0.37)
C0	3.89 (0.09)	25.25 (2.06)	16.84 (1.29)	5.85 (1.29)	1.05 (0.61)	1.02 (0.54)
C10	4.01 (0.17)	23.50 (6.24)	15.42 (2.19)	5.28 (1.86)	1.61 (1.42)	1.53 (0.53)
C15	3.98 (0.09)	21.00 (1.63)	13.78 (3.80)	5.73 (0.67)	1.16 (0.43)	1.33 (0.17)
C20	3.99 (0.10)	20.50 (2.08)	15.62 (2.60)	5.90 (1.25)	1.30 (0.49)	1.76 (0.46)

pH = in $CaCl_2$. OC = organic carbon content (Walkley-Black method). H+Al = potential acidity. Al^{3+}, Ca^{2+} and Mg^{2+} = exchangeable aluminum, calcium and magnesium. n represents the number of repetitions and values between parentheses represent the standard deviation

remaining under no-till system (NTS). Lime rates of 0 t ha^{-1} (C0), 10 t ha^{-1} (C10) 15 t ha^{-1} (C15), and 20 t ha^{-1} (C20) were applied on the NTS soil surface, without disturbing the soil. The lime used had 285 and 200 g kg^{-1} of CaO and MgO, and 100.6, 74.7, and 75.1% neutralizing power, reactivity, and total neutralizing relative power, respectively.

Thirty months after lime application, during bean flowering, four different locations per stripe were chosen to collect the disturbed soil samples, so that spatial variability was appropriately covered, at 0–10 cm (A) and 10–20 cm (B) soil layers. More details about the history of crop rotation adopted for the experiment under study can be found in Auler et al. (2017).

2.2 Soil analyses

2.2.1 Chemical attributes

Prior to chemical analysis, the soil samples were dried in forced air circulation oven (40 °C/48 h) and ground to pass through a 2-mm sieve. Soil organic carbon (OC) was determined by the Walkley-Black method according to Brazilian

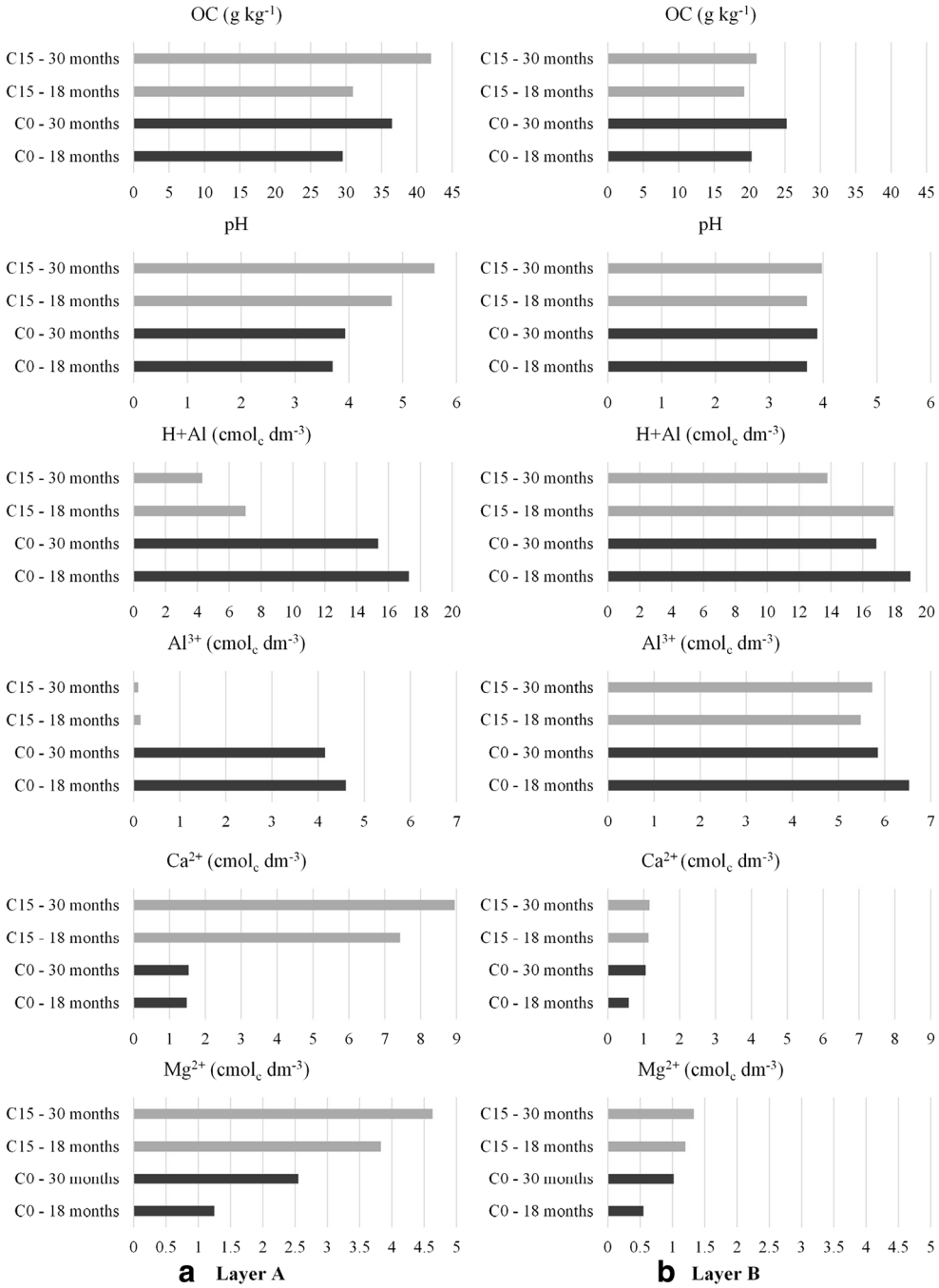

Fig. 1 Comparison of soil chemical attributes after 18 (Auler et al. 2017) and 30 months of lime application at **a** 0–10 cm (A) and **b** 10–20 cm (B) soil layers. For this comparison, only C0 and C15 were considered

guidelines reported in van Raij et al. (2001). Soil pH (active soil acidity) was determined in a 0.01 mol L^{-1} $CaCl_2$ suspension (1:2.5 soil/solution, *v/v*).

The potential acidity (H+Al) was determined by a SMP buffer procedure and exchangeable Al^{3+}, Ca^{2+}, and Mg^{2+} were extracted with neutral 1 mol L^{-1} KCl (1:10 soil/solution, *v/v*), according to standard methods described in Pavan et al. (1992). Exchangeable Al^{3+} (exchangeable acidity) was determined by titrating with 0.025 mol L^{-1} NaOH solution, Ca^{2+} and Mg^{2+} by titrating with 0.025 mol L^{-1} EDTA.

2.2.2 X-ray fluorescence technique

Semi-quantitative elemental analyses of the soil samples were performed through an energy dispersive X-ray fluorescence (XRF) spectrometer model EDX-720 (Shimadzu), equipped with an Rh X-ray tube. The equipment voltage varied from 5 to 50 kV and its tube current from 1 to 1000 μA. The system detector was a Si(Li) semi-conductor cooled with liquid N at − 196 °C. Standard procedures of calibration were performed whenever necessary (Pires et al. 2016).

Three measurement repetitions were carried with sample portions (~ 2 g containing equal aliquots from the four original samples for each stripe and soil layer) powdered and reduced to diameters lower than 45 μm which were placed into proper sample analysis cups covered with Mylar film (6 μm thickness). The measuring time for each sample was 100 s in Na-Sc (15 kV) and Ti-U (50 kV) energy bands. Measurements were performed under 30 Pa pressure and the spectral output was acquired in terms of oxides.

2.2.3 Attenuation parameters

The computer code XCOM, available in a web version supported by the National Institute of Standards and Technology, was used to compute the soil mass-absorption coefficients, $\mu_m = \mu/\rho$ (cm^2 g^{-1}), where μ is the linear absorption coefficient (cm^{-1}) and ρ is the soil bulk density (g cm^{-3}). For that, the oxide composition obtained from XRF analyses was taken as input data.

Photon energies related to the most common radioisotopes used as sources for γ-ray attenuation experimental investigations were selected for this study: 59.5 keV (^{241}Am) and 661.6 keV (^{137}Cs) (Corey et al. 1971; Reginato 1974; Ferreira and Pires 2016).

Contents of soil pH, OC, H+Al, Al^{3+}, Ca^{2+}, and Mg^{2+} were plotted against values of μ_m and a second-degree polynomial mathematical function was used to fit the data. Additionally, analyses of linear correlation were performed between values of μ_m and oxide mixtures aiming to determine if μ_m variations can be mostly explained by variations in the proportions of particular soil oxides.

For each studied photon energy, XCOM also provided the contribution of the incoherent scattering (is), coherent

Table 2 Energy dispersive XRF analysis for 0–10 cm (A) and 10–20 cm (B) soil layers ($n = 3$)

	Oxides (g kg^{-1})									
	SiO_2	Al_2O_3	CaO	Fe_2O_3	K_2O	SO_3	TiO_2	MnO	ZrO_2	ZnO	Rb_2O
Layer A											
Ref.	608.88 (1.22)	299.93 (3.56)	–	52.93 (1.43)	15.57 (0.40)	12.69 (0.39)	9.01 (0.22)	0.41 (0.03)	0.38 (0.02)	0.08 (0.01)	0.11 (0.00)
C0	605.36 (0.55)	307.81 (0.75)	–	51.03 (1.06)	15.20 (0.13)	11.21 (0.13)	8.73 (0.13)	0.33 (0.02)	0.19 (0.02)	0.06 (0.00)	0.07 (0.00)
C10	609.71 (1.40)	291.52 (3.84)	8.50 (0.58)	52.08 (0.43)	14.73 (0.31)	13.47 (1.63)	8.84 (0.05)	0.69 (0.01)	0.27 (0.01)	0.08 (0.00)	0.09 (0.00)
C15	599.04 (1.52)	291.89 (2.06)	22.69 (0.63)	50.34 (0.46)	14.16 (0.74)	12.33 (0.15)	8.48 (0.09)	0.60 (0.02)	0.28 (0.01)	0.07 (0.00)	0.10 (0.01)
C20	582.85 (2.22)	262.33 (4.70)	68.71 (2.20)	48.09 (0.64)	14.16 (0.09)	14.06 (1.58)	8.72 (0.10)	0.67 (0.02)	0.24 (0.03)	0.08 (0.01)	0.08 (0.00)
Layer B											
Ref.	575.81 (1.52)	328.32 (2.02)	–	57.72 (0.62)	15.84 (0.05)	12.14 (0.55)	9.50 (0.12)	0.29 (0.02)	0.23 (0.02)	0.07 (0.01)	0.08 (0.01)
C0	593.73 (1.92)	316.11 (2.76)	–	54.10 (0.68)	15.18 (0.08)	11.47 (0.51)	8.59 (0.09)	0.27 (0.02)	0.34 (0.01)	0.06 (0.00)	0.12 (0.01)
C10	593.30 (0.18)	314.62 (0.32)	–	55.40 (0.37)	14.66 (0.03)	12.07 (0.56)	8.93 (0.06)	0.30 (0.02)	0.34 (0.02)	0.06 (0.00)	0.11 (0.01)
C15	585.61 (2.49)	327.22 (2.52)	–	52.82 (0.31)	14.86 (0.26)	9.78 (0.11)	9.05 (0.08)	0.26 (0.04)	0.23 (0.00)	0.06 (0.01)	0.08 (0.00)
C20	593.54 (4.47)	322.86 (3.96)	–	49.33 (0.52)	14.71 (0.13)	10.02 (0.53)	9.01 (0.08)	0.24 (0.02)	0.17 (0.02)	0.06 (0.01)	0.06 (0.01)

Oxides contributing with less than 0.005 g kg^{-1} were disregarded. n represents the number of repetitions and values between parentheses represent the standard deviation

scattering (cs), photoelectric absorption (pa), and pair production (pp) in μ_m (Berger and Hubbell 1987):

$$\mu_m = \mu_{m\ is} + \mu_{m\ cs} + \mu_{m\ pa} + \mu_{m\ pp}, \quad (1)$$

The μ_m values were also used to determine the total molecular cross section (σ_m) as follows (Akça and Erzeneoğlu 2014):

$$\sigma_m = (\mu_m)\left(\frac{M}{N_A}\right), \quad (2)$$

where $M = \sum_i n_i A_i$ is the molecular weight of the compound, N_A is Avogadro's number, A_i is the atomic weight of the ith element and n_i is the number of formula units in the molecule.

The average atomic and electronic cross sections (σ_a and σ_e) were in turn obtained through (Han and Demir 2009):

$$\sigma_a = \frac{\sigma_m}{\sum_i n_i}, \quad (3)$$

$$\sigma_e = \frac{1}{N_A}\sum_i \frac{f_i A_i}{Z_i}(\mu_m)_i, \quad (4)$$

where $\sum_i n_i$ is the total number of formula units; $f_i = n_i/\sum_j n_j$ and Z_i are fractional abundance and atomic number of the constituent element, n_j is the number of atoms of the constituent element, and $\sum_j n_j$ is the total number of atoms present in the molecular formula.

The effective atomic number (Z_{eff}) was obtained by relating the Eqs. (2), (3), and (4) (Han and Demir 2009; Akça and Erzeneoğlu 2014):

$$\sigma_m = \sigma_a \sum_i n_i = Z_{eff}\sigma_e \sum_i n_i, \quad (5)$$

$$\therefore Z_{eff} = \frac{\sigma_a}{\sigma_e}, \quad (6)$$

Finally, the effective electron number or electron density (number of electrons per unit mass) was calculated by (Medhat et al. 2014):

$$N_{el} = \frac{\mu_m}{\sigma_e}. \quad (7)$$

Values of μ_m along with percentage contributions of *cs*, *is* and *pa*, σ_a, σ_e, Z_{eff}, and N_{el} were plotted as function of soil lime treatments (C0, C10, C15, and C20) and Ref., for ^{241}Am and ^{137}Cs. In addition, the variation of μ_m, Z_{eff}, and N_{el} (plus the behavior of Z_{eff} versus N_{el}), as function of the photon energy (40–661.6 keV), was graphically presented with power, logarithmic, and linear fittings.

2.2.4 Prediction of soil physical properties

When a gamma-ray beam of incident intensity I_0 (cps) interacts with a soil of thickness x, the transmitted intensity I (cps) through the absorber follows the Beer-Lambert law (Pires and Pereira 2014):

$$I = I_0 e^{-\mu_m \rho x}. \quad (8)$$

Therefore, the values of μ_m obtained in the present study, together with fixed values of I (62,035 cps), I_0 (506,458 cps), and x (6.027 cm), which were extracted from a previous study performed with a soil of similar elemental composition (Pires et al. 2014), were used to predict the soil bulk density (ρ) and total porosity (φ) as follows:

$$\rho = \frac{1}{\mu_m x}\ln\frac{I_0}{I}, \quad (9)$$

$$\varphi = 1 - \frac{\rho}{\rho_p}. \quad (10)$$

where ρ_p is the soil particle density which was determined with an Helium gas multipycnometer (model MVP-D160-E, Quantachrome Instruments). The average ρ_p values obtained for layers A and B were 2.38 and 2.47 g cm^{-3}, respectively.

3 Results and discussion

Comparing C10, C15, and C20 to Ref. and C0 (Table 1), it is notable that surface liming increased contents of soil pH, Ca^{2+}, and Mg^{2+}, while reduced H+Al and Al^{3+} at layer A. Nevertheless, at layer B, chemical attributes did not undergo as pronounced variations. The less successful effect of liming to correct soil acidity at the subsurface layer is due to the slow natural mobility of lime through the soil depth related to the low solubility of agricultural limestones (Ernani et al. 2004).

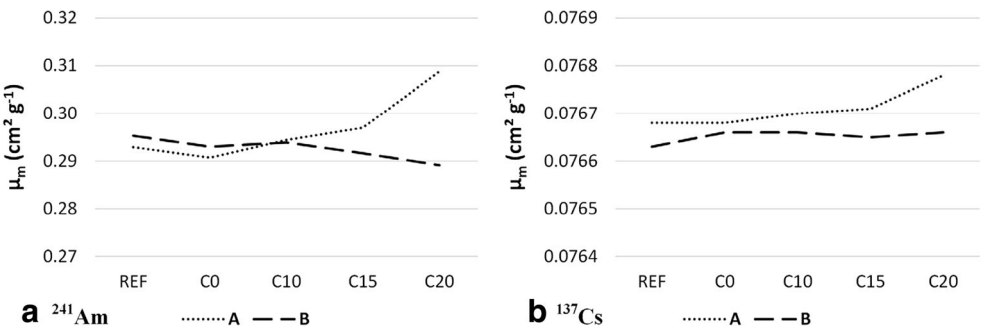

Fig. 2 Soil mass attenuation coefficients (μ_m) obtained through XCOM as function of the soil treatments (Ref., C0, C10, C15, and C20) at 0–10 cm (A) and 10–20 cm (B) soil layers for **a** ^{241}Am and **b** ^{137}Cs photon energies

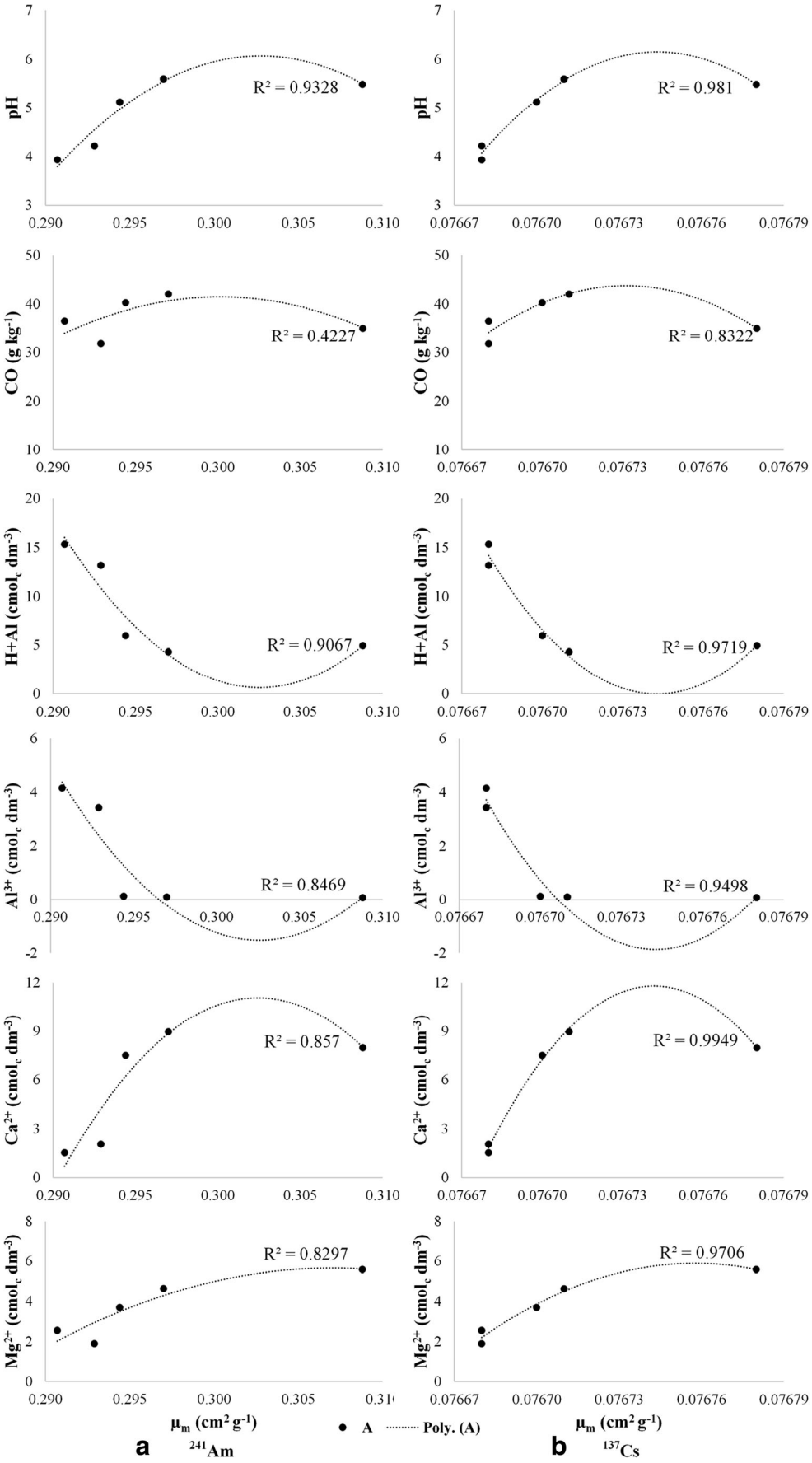

Fig. 3 Soil chemical attributes correlated to mass attenuation coefficients (μ_m) by a second-degree polynomial mathematical model at 0–10 cm (A) layer under soil treatments: Ref, C0, C10, C15, and C20 for **a** ^{241}Am and **b** ^{137}Cs photon energies. R^2 stands for the coefficient of determination

Table 3 Simple linear correlation coefficients of Pearson (r) between individual contribution of soil oxides and mass attenuation coefficients (μ_m) determined with ^{241}Am and ^{137}Cs photon energies for 0–10 cm (A) and 10–20 cm (B) soil layers

	Layer A		Layer B	
Oxides (g kg^{-1})	$r_{\mu(241Am)}$	$r_{\mu(137Cs)}$	$r_{\mu(241Am)}$	$r_{\mu(137Cs)}$
SiO_2	− 0.942	− 0.945	− 0.549	*0.993*
Al_2O_3	− 0.986	− 0.981	− 0.053	− 0.762
CaO	*0.993*	*0.996*	–	–
Fe_2O_3	− 0.861	− 0.894	*0.996*	− 0.644
K_2O	− 0.733	− 0.765	0.668	− 0.862
SO_3	0.757	0.735	0.875	− 0.309
TiO_2	− 0.281	− 0.325	0.321	− 0.873
MnO	0.664	0.678	0.915	− 0.314
ZrO_2	− 0.143	− 0.253	0.580	0.304
ZnO	0.545	0.499	0.854	− 0.783
Rb_2O	− 0.254	− 0.356	0.583	0.296

Higher values of r are indicated in italic

At both soil layers, no effect of management alone can be inferred from the results since only slight changes occurred between Ref. (pasture area) and C0 (no-till system without liming), regarding all chemical attributes.

An investigation concerning effects of surface and incorporated liming on physical-hydrical attributes of the same soil under study in this work, after 18 months of lime application, is found in Auler et al. (2017). For each application manner, the mentioned investigation considered only 0 and 15 t ha^{-1} (calculated to raise the base saturation at the 0–20-cm soil layer to 70%) lime rates, respectively equivalent to C0 and C15. Twelve months after this evaluation, totalizing 30 months of lime application, most of the chemical attributes undergone greater changes for C15 in relation to C0 at the top soil layer (Fig. 1a). This is an indicative that variations in soil chemical attributes after the 30-month period is not only due to crop rotation, whose effects are exclusively seen in C0, but it is still strongly related to lime reaction.

At layer B, from 18 to 30 months, C0 and C15 (Fig. 1b) presented much more subtle effects than at layer A (Fig. 1a). Besides, at this soil depth, only reduction of H+Al content is

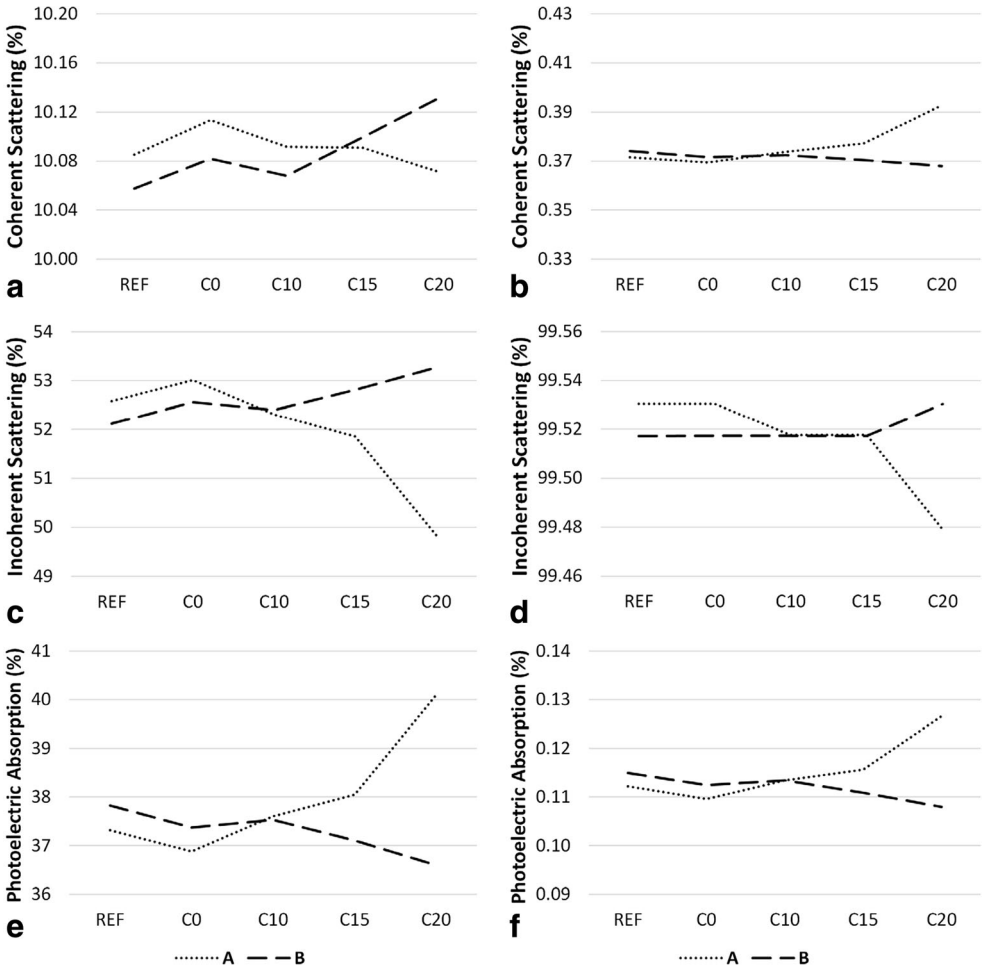

Fig. 4 Percentage contributions of coherent scattering, incoherent scattering, and photoelectric absorption to the computation of the mass attenuation coefficients (μ_m) as function of the soil treatments (Ref, C0, C10, C15, and C20) at 0–10 cm (A) and 10–20 cm (B) soil layers for ^{241}Am (**a**, **c**, **e**) and ^{137}Cs (**b**, **d**, **f**) photon energies

more pronounced for C15 in relation to C0, which indicates that soil acidity components were not remarkably ameliorated at the subsurface layer in the course of time. Similar results regarding effects of liming on soil chemical attributes, over a period of 4 years, at the 0–5, 5–10, 10–20, and 20–40 cm soil depths are found in Caires et al. (2006).

Rheinheimer et al. (2000) developed a study considering lime rates of 0.0, 2.0, 8.5, and 17 Mg ha^{-1} superficially applied and incorporated to a soil from south Brazil. These authors reported that the soil acidity correction at the top layer was proportional to the lime rate, independent of the application manner. However, greater values of soil pH, OC, and Ca^{2+} as well as lower values of H+Al and Al^{3+} were observed for C15 instead of C20, at layer A (Table 1). This indicates that the highest lime rate did not promote further soil chemical amelioration beyond the intermediary rate.

Among soil constituent oxides, SiO_2, Al_2O_3, and Fe_2O_3 are predominant (Garrison 2008) (Table 2). Considering that CaO was not identified for neither Ref. and C0 at layer A nor for any treatment at layer B, it is reasonable to say that this particular oxide is not inherent to this soil. Inceptisols classified as Dystrudept, such as the soil under investigation, are indeed base-poor due to its acid parent material (Hudnall 2011). Therefore, the appearance of CaO at layer A is most likely exclusively due to liming and, as it would be expected, its contribution increases with the increase in the lime rate. In

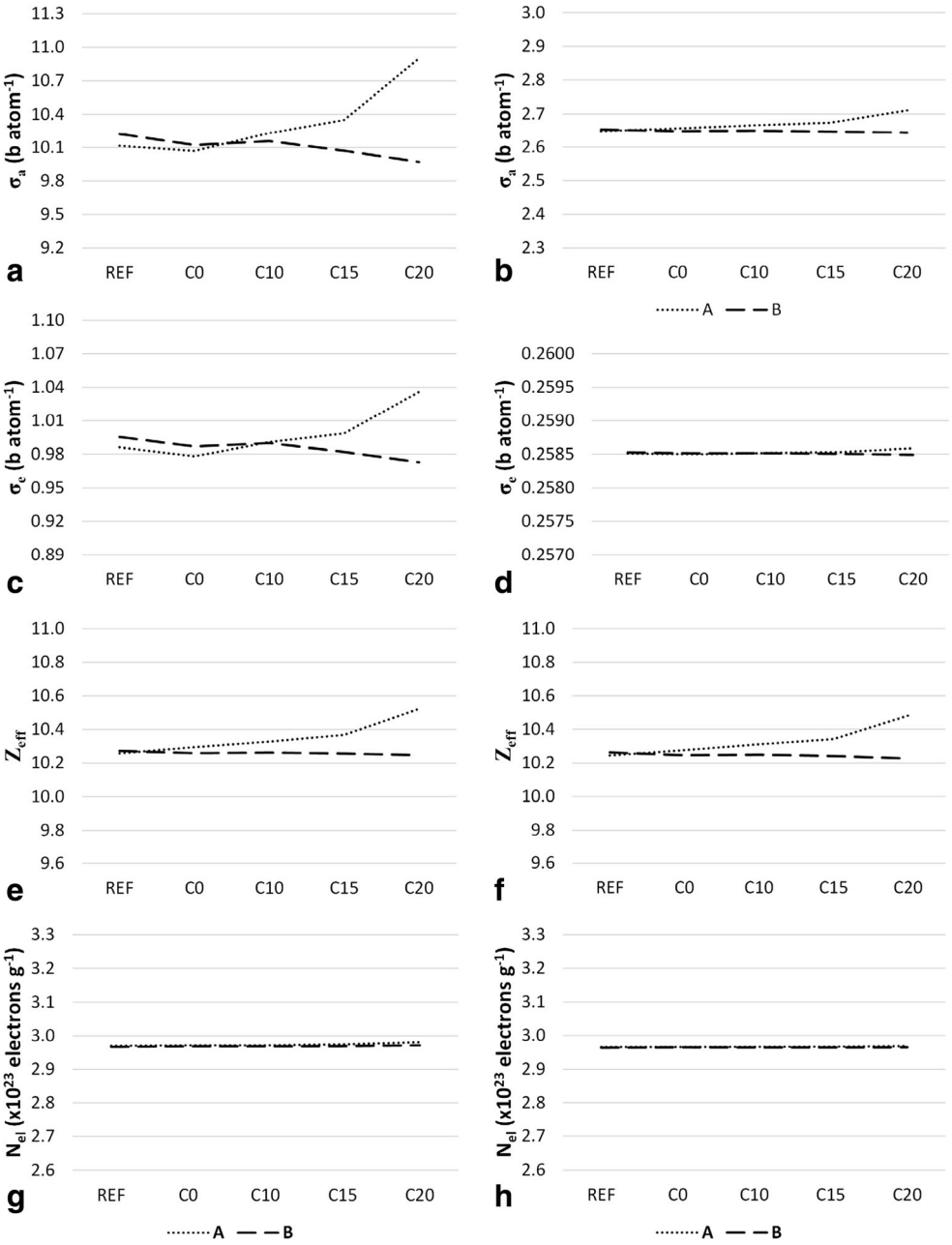

Fig. 5 Average atomic and electronic cross sections (σ_a and σ_e), effective atomic number (Z_{eff}), and effective electron density (N_{el}) as function of the soil treatments (Ref, C0, C10, C15, and C20) at 0–10 cm (A) and 10–20 cm (B) soil layers for ^{241}Am (**a**, **c**, **e**, **g**) and ^{137}Cs (**b**, **d**, **f**, **h**) photon energies

virtue of the slow mobility of lime through the soil depth, CaO have not reached the soil subsurface layer in sufficient amount to be detected by XRF technique.

It is known that low energy photons have more pronounced interaction with the matter in comparison to the high energy ones (Rangacharyulu 2014). For this reason, lower values of μ_m were obtained using the higher photon energy of ^{137}Cs (Fig. 2b). The μ_m values shown in Fig. 2 are in agreement to the findings of Pires et al. (2016) (^{241}Am: 0.26–0.30 cm^2 g^{-1} and ^{137}Cs: 0.0764–0.0765 cm^2 g^{-1}) concerning different Brazilian hardsetting soils. As can be seen from Fig. 2, μ_m increases with the increasing in the lime rate at layer A, considering both sources. At layer B, though, μ_m values kept practically constant among treatments regardless the photon energy.

Chemical attributes from layer A (Table 1) plotted against data of μ_m (calculated for ^{241}Am and ^{137}Cs photon energies) for Ref. and lime treatments (Fig. 2) resulted in curves which were in most cases well fitted by a second-degree polynomial mathematical model (Fig. 3). For both sources, better adjustments were found for contents of soil pH, H+Al, and Ca^{2+}, which indicates that μ_m variation is in fact related to the effects of liming.

Among all chemical parameters evaluated, OC seem to play a less important role in the increasing of μ_m (Fig. 3). The soil OC is an indirect parameter to evaluate the content of soil organic matter but it measures only the carbon contribution (Baldock and Broos 2011), which, for being a light element, weakly influences μ_m. At layer B, neither polynomial nor linear adjustments fitted well to the data, suggesting that variation on soil chemical attributes and μ_m cannot be associated at this soil depth.

Linear correlation analysis between soil constituent oxides (Table 2) and μ_m values obtained for each soil treatment (Fig. 2) also provides evidence that, at layer A, the increase in μ_m is more strongly related to the increasing amount of CaO in the soil (Table 3). At this same layer, the correlation coefficients from ^{241}Am and ^{137}Cs photon energies are more alike in comparison to layer B. This happens probably because μ_m variation at layer B (Fig. 2) presents an inverse behavior when comparing results for the two different energies, i.e., while μ_m slightly diminishes for ^{241}Am, it slightly increases for ^{137}Cs. Therefore, at layer B, the decrease in μ_m for the ^{241}Am photon energy is mostly due to the reduction in Fe_2O_3, which is in line with results of Pires et al. (2016), and the increase in μ_m for ^{137}Cs is governed by the increase in SiO_2 (Table 3).

It is notable from Fig. 4 that the incoherent scattering is the dominant process by which the radiation interacts with matter, mainly for ^{137}Cs (~ 99.5% of the radiation interaction). Incoherent scattering in fact dominates over the remaining processes when the incident photon energy is in an intermediary energy range ~ 100 keV to ~ 1 MeV (Kucuk et al. 2013). On the other hand, considering the lower characteristic photon energy of ^{241}Am, the incoherent scattering contribution drops to about half of the total contribution (Fig. 4c) and substantial percentages of photoelectric absorption (Fig. 4e) and coherent scattering (Fig. 4a) take place.

Incoherent scattering cross section is weakly influenced by the chemical composition of the target because it has linear dependence on Z. The photoelectric and coherent cross sections, on the other hand, are more strongly dependent on the atomic number of the constituent elements ($Z^{4–5}$ and $Z^{2–3}$, respectively) (Medhat et al. 2014). Thus, taking into account the variations in chemical composition among treatments, the greater changes in μ_m found for ^{241}Am in comparison to ^{137}Cs (Fig. 2) are justified by the differences regarding the contributions of scattering and absorption processes between the considered photon energies (Fig. 4).

The assumption that the original atoms in a given molecule or compound could be replaced by an equivalent number of average atoms, each of which having the same average atomic number, leads to the idea of the effective atomic number (Z_{eff}) (Manohara et al. 2010). Z_{eff} depends not only on the atomic numbers of the various composite material elements and its relative proportion but also on the number of elements present in it (Mudahar and Sahota 1988; Baltaş and Çevik 2008). A demonstration of the dependence of Z_{eff} on the chemical composition of amino acids is found in the study of Manohara and Hanagodimath (2007).

Table 4 Fractional abundance ($f_O + f_{Al} + \ldots + f_{Zn} = 1$) of constituent soil elements for 0–10 cm (A) and 10–20 cm (B) soil layers

	Fractional abundance				
	Ref.	C0	C10	C15	C20
Layer A					
O (8)	0.495	0.496	0.494	0.491	0.483
Si (14)	0.285	0.283	0.285	0.280	0.272
Al (13)	0.159	0.163	0.154	0.154	0.139
Ca (20)	–	–	0.006	0.016	0.049
Fe (26)	0.037	0.036	0.036	0.035	0.034
K (19)	0.013	0.013	0.012	0.012	0.012
S (16)	0.005	0.004	0.005	0.005	0.006
Ti (22)	0.005	0.005	0.005	0.005	0.005
Layer B					
O (8)	0.492	0.494	0.494	0.494	0.495
Si (14)	0.269	0.278	0.277	0.274	0.277
Al (13)	0.174	0.167	0.167	0.173	0.171
Ca (20)	0.040	0.038	0.039	0.037	0.035
Fe (26)	0.013	0.013	0.012	0.012	0.012
K (19)	0.005	0.005	0.005	0.004	0.004
S (16)	0.006	0.005	0.005	0.005	0.005

Values between parentheses represent the atomic number of each element. The fractional abundance of Mn (25), Zr (40), Zn (30) and Rb (37) correspond to less than 0.001

The current soil under study has in its composition elements with atomic number varying from 8 (O) to 40 (Zr) and, as expected, Z_{eff} lies within this interval (Fig. 5e, f). However, Z_{eff} is inversely dependent on the sum over the fractional abundance (f) of each soil constituent element (see Eqs. 4 and 6) and the elements that present higher f are O (8), Si (14), and Al (13) (Table 4). For this reason, Z_{eff} is closer to the inferior limit of the Z variation in the soil.

As the variety of soil constituent elements increase when Ca starts being computed (Table 4) due to the lime rates, at layer A, Z_{eff} also increases (Fig. 5e, f). Thus, at this layer, the increase of photoelectric absorption (Fig. 4e, f) and consequent decrease in incoherent scattering (Fig. 4c, d) contributions with lime treatments can be related to the increase in Z_{eff} (Önder et al. 2012). This is because of the much stronger dependence on Z of photoelectric absorption in comparison to the incoherent scattering (Kaplan 1977). At layer B, it can be considered from the plot scale that Z_{eff} kept rather constant among treatments and consequently slighter changes are seen for percentages of radiation interaction.

From Fig. 5, one can see that the trend behavior of all attenuation parameters (σ_a, σ_e, Z_{eff}, and N_{el}) is practically the same for the two photon energies. Nevertheless, the variation of these parameters is smaller for ^{137}Cs than for ^{241}Am due to the total dominance of incoherent scattering in the former and broader contribution of photoelectric absorption in the last (Fig. 4). Both atomic and electronic cross sections increase with the increasing in the lime rate, meaning that the limed soil samples present a higher probability to attenuate the gamma-ray photons, in accordance with the variation in μ_m (Fig. 2) (Eisberg 1885).

Figure 6 portraits how μ_m, Z_{eff}, and N_{el} vary from 40 to 661.6 keV. It is possible to see that over this energy range, μ_m goes from about 0.60 to under 0.10 cm^2 g^{-1} in a power law

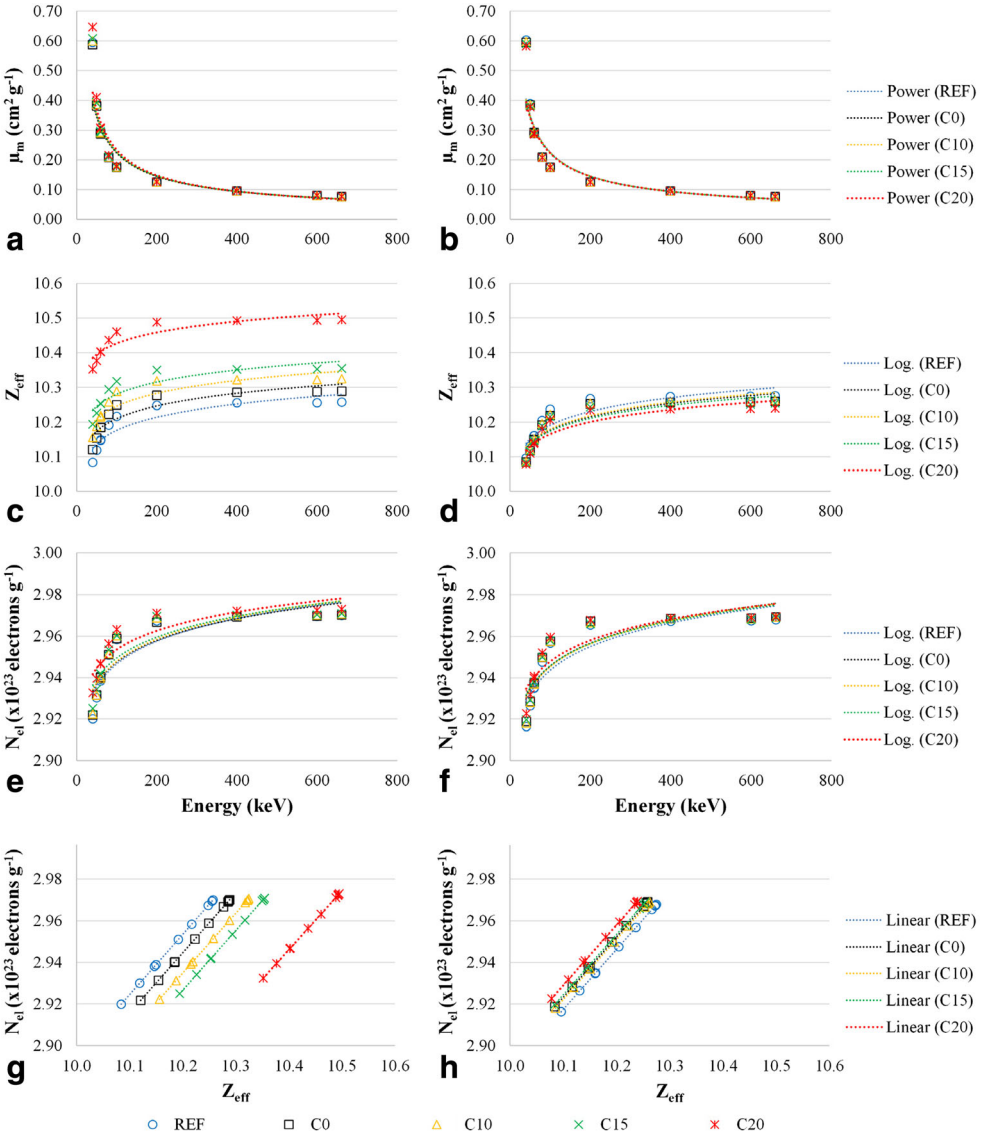

Fig. 6 Variation of mass attenuation coefficients (μ_m), effective atomic number (Z_{eff}), and effective electron density (N_{el}) as function of the photon energy (E) (40–661.6 keV) with power and logarithmic adjustments. N_{el} variation as function of Z_{eff}, with linear adjustment, over the same energy range at 0–10 cm (A) (**a**, **c**, **e**, **g**) and 10–20 cm (B) (**b**, **d**, **f**, **h**) soil layers

Table 5 Parameters of power adjustment for mass attenuation coefficients (μ_m) and logarithmic adjustment for effective atomic number (Z_{eff}) and effective electron density (N_{el}) plotted as function of the energy (E) (40–661.6 keV); linear adjustment for N_{el} plotted as function of Z_{eff} in the same energy range, considering the 0–10 cm (A) and 10–20 cm (B) soil layers. R^2 stands for the coefficient of determination

	Layer A			Layer B		
	a	b	R^2	a	b	R^2
Power fit: $\mu_m = aE^b$						
REF	4.097	− 0.631	0.926	4.206	− 0.635	0.926
C0	4.002	− 0.627	0.927	4.103	− 0.631	0.926
C10	4.161	− 0.633	0.926	4.141	− 0.632	0.926
C15	4.270	− 0.637	0.925	4.045	− 0.628	0.927
C20	4.799	− 0.656	0.923	3.940	− 0.624	0.927
Logarithmic fit: $Z_{eff} = aln(E) + b$						
REF	0.054	9.926	0.822	0.057	9.930	0.820
C0	0.052	9.970	0.827	0.055	9.923	0.818
C10	0.053	10.000	0.816	0.056	9.924	0.816
C15	0.050	10.048	0.815	0.053	9.928	0.819
C20	0.046	10.215	0.830	0.051	9.933	0.806
Logarithmic fit: $N_{el} = aln(E) + b$						
REF	0.016	2.287	0.822	0.016	2.868	0.820
C0	0.015	2.878	0.827	0.016	2.872	0.818
C10	0.015	2.877	0.816	0.016	2.871	0.816
C15	0.015	2.883	0.815	0.015	2.875	0.819
C20	0.013	2.894	0.830	0.015	2.880	0.806
Linear fit: $N_{el} = aZ_{eff} + b$						
REF	0.290	-2.10^{-11}	1.000	0.289	-9.10^{-12}	1.000
C0	0.289	-1.10^{-11}	1.000	0.289	-2.10^{-11}	1.000
C10	0.288	0.000	1.000	0.289	4.10^{-11}	1.000
C15	0.287	0.000	1.000	0.290	3.10^{-11}	1.000
C20	0.283	-7.10^{-11}	1.000	0.290	-2.10^{-11}	1.000

(Fig. 6a, b; Table 5) and the variation due to treatments is more evident at lower energies, as seen also in Fig. 2.

For all treatments, Z_{eff} undergoes a sharp increase from 40 to 200 keV and then its increasing turns smoother, which is well represented by a logarithmic function (Fig. 6c, d; Table 5). The Z_{eff} behavior described here is very similar to the one presented in Medhat et al. (2014), within the same energy interval, for eight soils from the Southeast and South of Brazil. Among treatments, though, differences in Z_{eff} are not magnified at low or high energy regions, but on the contrary remain almost the same over the entire range (Fig. 6c, d).

Just like Z_{eff}, N_{el} varies logarithmically with the energy, as seen in Fig. 6e, f and Table 5. Several studies such as those performed by Baltaş and Çevik (2008), Medhat (2011), and Marashdeh et al. (2015) report that Z_{eff} and N_{el} present indeed similar dependence on photon energy. This was confirmed by plotting these two important attenuation parameters against each other (Fig. 6g, h), which resulted in a linear relation (Table 5). It is worth to mention that the plot scales in Fig. 6 were zoomed in relation to Fig. 5 in order to better visualize variations in N_{el} and Z_{eff}.

Finally, it is notable that although the variation in μ_m among treatments is subtle, when using ^{247}Am photon energy, it causes relevant variation in ρ and φ, in the sense that a higher μ_m gives lower ρ_s and higher φ (layer A) and vice versa (layer B) (Table 6). On the other hand, μ_m values obtained with ^{137}Cs photon energy practically did not change ρ_s and φ at neither of the soil layers. This occurs due to the weak interaction of the photon with the soil for this specific energy, which explains the similarities in μ_m values (Pires and Pereira 2014; Pires et al. 2016).

With these results in mind, one should be aware that using a unique attenuation coefficient, in order to determine ρ_s and φ of a soil submitted to different lime rates, may over or underestimate these important soil physical properties, especially when the chosen energy source is ^{247}Am.

These findings are relevant because traditionally, in the soil science area, μ_m values are calculated without considering any chemical modification to which the soil can be submitted. As

Table 6 Values of soil bulk density (ρ_s) and total porosity (φ) predicted based on mass attenuation coefficients (μ_m) determined with ^{241}Am and ^{137}Cs photon energies for 0–10 cm (A) and 10–20 cm (B) soil layers of the Dystrudept

	Layer A			Layer B		
	μ_m ($cm^2\ g^{-1}$)	ρ ($g\ cm^{-3}$)	Φ ($cm^3\ cm^{-3}$)	μ ($cm^2\ g^{-1}$)	ρ ($g\ cm^{-3}$)	Φ ($cm^3\ cm^{-3}$)
^{247}Am						
REF	0.2929	1.190	0.502	0.2953	1.180	0.523
C0	0.2907	1.199	0.498	0.2930	1.189	0.520
C10	0.2944	1.183	0.504	0.2939	1.185	0.521
C15	0.2970	1.173	0.509	0.2916	1.195	0.517
C20	0.3088	1.128	0.526	0.2891	1.205	0.513
^{137}Cs						
REF	0.07668	1.236	0.482	0.07663	1.237	0.500
C0	0.07668	1.236	0.482	0.07666	1.237	0.501
C10	0.07670	1.236	0.482	0.07666	1.237	0.501
C15	0.07671	1.236	0.482	0.07665	1.237	0.500
C20	0.07678	1.235	0.483	0.07666	1.237	0.501

the soil bulk density and its total porosity are important parameters from the agricultural and environmental points of view, not representative measurements of μ_m can lead to biased values of ρ_s and φ as shown (Pires and Medhat 2016).

4 Conclusions

1. Thirty months after liming application in the soil surface, substantial improvements of chemical attributes were achieved at the top soil layer, reflecting reduction in soil acidity. However, this procedure was not efficient to correct soil acidity at the subsoil;
2. Liming increased the soil attenuation parameters (mass attenuation coefficient, atomic and electronic cross sections, effective atomic number and electron density) at the surface layer but practically did not change them at the subsurface;
3. The increasing in the soil attenuation parameters was more accentuated when using the ^{241}Am photon energy in comparison to ^{137}Cs due to the higher contribution of photoelectric absorption in the former;
4. The determination of soil physical properties such as bulk density and total porosity is more influenced by variation of mass attenuation coefficients computed with ^{241}Am than ^{137}Cs photon energy.

Acknowledgements We would like to thank Dr. José A. Baptista from IAPAR and the farmers for making the experimental area available.

Funding information The authors acknowledge CNPq ("Conselho Nacional de Desenvolvimento Científico e Tecnológico") for the research grant for Dr. L.F. Pires (303726/2015-6) and CAPES ("Coordenação de Aperfeiçoamento de Pessoal de Nível Superior") for the PhD grant for MS. T.R. Ferreira and MS. A.C. Auler.

References

Akça B, Erzeneoğlu SZ (2014) The mass attenuation coefficients, electronic, atomic, and molecular cross sections, effective atomic numbers, and electron densities for compounds of some biomedically important elements at 59.5 keV. Sci Technol Nucl Install 2014:1–8

Auler AC, Pires LF, dos Santos JAB, Caires EF, Borges JAR, Giarola NFB (2017) Effects of surface-applied and soil-incorporated lime on some physical attributes of a Dystrudept soil. Soil Use Manag 33: 129–140

Baldock JA, Broos K (2011) Soil organic matter. In: Huang PM, Li Y, Sumner ME (eds) Handbook of soil sciences properties and processes—part II: soil chemistry. CRC Press, Boca Raton, pp 11.1–11.52

Baltaş H, Çevik U (2008) Determination of the effective atomic numbers and electron densities for YBaCuO superconductor in the range 59.5–136keV. Nucl Instrum Methods Phys Res Sect B Beam Interact Mater Atoms 266:1127–1131

Berger MJ, Hubbell JH (1987) XCOM: photon cross sections on a personal computer, NBSIR 87–3597. National Bureau of Standards, USA

Caires EF, Barth G, Garbuio FJ (2006) Lime application in the establishment of a no-till system for grain crop production in southern Brazil. Soil Tillage Res 89:3–12

Corey JC, Peterson SF, Wakat MA (1971) Measurement of attenuation of 137Cs and 241Am gamma rays for soil density and water content determinations. Soil Sci Soc Am J 35:215

Costa JC, Borges JAR, Pires LF (2013) Soil bulk density evaluated by gamma-ray attenuation: analysis of system geometry. Soil Till Res 129:23–31

Demir D, Ün A, Özgül M, Şahin Y (2008) Determination of photon attenuation coefficient, porosity and field capacity of soil by gamma-ray transmission for 60, 356 and 662keV gamma rays. Appl Radiat Isot 66:1834–1837

Eisberg R (1885) Cross sections for photon absorption and scattering. In: Quantum physics of atoms, molecules, solids, nuclei, and particles, 2nd edn. Wiley, New York, pp 48–54

Ernani PR, Ribeiro MFS, Bayer C (2004) Chemical modifications caused by liming below the limed layer in a predominantly variable charge acid soil. Commun Soil Sci Plant Anal 35:889–901

Ferreira TR, Pires LF (2016) Soil porosity distribution representative elementary area analyzed through gamma-ray computed tomography. Int Agrophysics. https://doi.org/10.1515/intag-2016-0016

Garrison S (2008) The chemistry of soils, second. Oxford University Press, New York

Gerward L, Guilbert N, Jensen KB, Levring H (2004) WinXCom—a program for calculating X-ray attenuation coefficients. Radiat Phys Chem 71:653–654

Han I, Demir L (2009) Determination of mass attenuation coefficients, effective atomic and electron numbers for Cr, Fe and Ni alloys at different energies. Nucl Instrum Methods Phys Res Sect B Beam Interact Mater Atoms 267:3–8

Haynes RJ, Naidu R (1998) Influence of lime, fertilizer and manure applications on soil organic matter content and soil physical conditions: a review. Nutr Cycl Agroecosyst 51:123–137

Hubbell JH (1969) Photon cross sections, attenuation coefficients, and energy absorption coefficients from 10 keV to 100 GeV, NSRDS-NBS 29. National Bureau of Standards, USA

Hudnall WH (2011) Classification of soils: Inceptisols. In: Huang PM, Li Y, Sumner ME (eds) Handbook of soil sciences properties and processes—part V: pedology, 2nd edn. CRC Press, Boca Raton, pp 63–71

Jones JBJ (2003) Agronomic handbook: management of crops, soils and their fertility. CRC Press, Boca Raton

Kaplan I (1977) Nuclear physics, 2nd edn. Addison-Wesley Press, Reading

Kucuk N, Tumsavas Z, Cakir M (2013) Determining photon energy absorption parameters for different soil samples. J Radiat Res 54:578–586

Manohara SR, Hanagodimath SM (2007) Studies on effective atomic numbers and electron densities of essential amino acids in the energy range 1keV–100GeV. Nucl Instrum Methods Phys Res Sect B Beam Interact Mater Atoms 258:321–328

Manohara SR, Hanagodimath SM, Thind KS, Gerward L (2010) The effective atomic number revisited in the light of modern photon-interaction cross-section databases. Appl Radiat Isot 68:784–787

Marashdeh MW, Al-Hamarneh IF, Abdel Munem EM et al (2015) Determining the mass attenuation coefficient, effective atomic number, and electron density of raw wood and binderless particleboards of *Rhizophora* spp. by using Monte Carlo simulation. Results Phys 5:228–234

Medhat ME (2011) Studies on effective atomic numbers and electron densities in different solid state track detectors in the energy range 1keV–100GeV. Ann Nucl Energy 38:1252–1263

Medhat ME, Pires LF, Arthur RCJ (2014) Analysis of photon interaction parameters as function of soil composition. J Radioanal Nucl Chem 300:1105–1112

Mora ML, Schnettler B, Demanet R (1999) Effect of liming and gypsum on soil chemistry, yield, and mineral composition of ryegrass grown in an acidic Andisol. Commun Soil Sci Plant Anal 30:1251–1266

Mudahar GS, Sahota HS (1988) Effective atomic number studies in different soils for total photon interaction in the energy region 10–5000 keV. Int J Radiat Appl Instrumentation Part A Appl Radiat Isot 39: 1251–1254

Önder P, Turşucu A, Demir D, Gürol A (2012) Studies on mass attenuation coefficient, effective atomic number and electron density of some thermoluminescent dosimetric compounds. Nucl Instrum Methods Phys Res Sect B Beam Interact Mater Atoms 292:1–10

Pavan MA, Bloch MF, Zempulski HC et al (1992) Manual de análise química do solo e controle de qualidade. Instituto Agronômico do Paraná (IAPAR), Londrina, BR

Pires LF, Medhat ME (2016) Different methods of mass attenuation coefficient evaluation: influences in the measurement of some soil physical properties. Appl Radiat Isot 111:66–74

Pires LF, Pereira ABP (2014) Gamma-ray attenuation to evaluate soil porosity: an analysis of methods. ScientificWorldJournal 2014: 723041

Pires LF, Bacchi OOS, Reichardt K (2005) Soil water retention curve determined by gamma-ray beam attenuation. Soil Tillage Res 82: 89–97

Pires LF, Rosa JA, Pereira AB et al (2009) Gamma-ray attenuation method as an efficient tool to investigate soil bulk density spatial variability. Ann Nucl Energy 36:1734–1739

Pires LF, Prandel LV, Saab SC (2014) The effect of wetting and drying cycles on soil chemical composition and their impact on bulk density evaluation: an analysis by using XCOM data and gamma-ray computed tomography. Geoderma 213:512–520

Pires LF, Brinatti AM, Prandel LV, da Costa Saab S (2016) Mineralogical composition of hardsetting soils and its effect on the radiation attenuation characteristics. J Soils Sediments 16:1059–1068

Rangacharyulu C (2014) Physics of nuclear radiations: concepts, techniques and applications. CRC Press, Boca Raton

Reginato RJ (1974) Gamma radiation measurements of bulk density changes in a soil Pedon following Irrigation1. Soil Sci Soc Am J 38:24

Rheinheimer DS, Santos EJS, Kaminski J et al (2000) Alterações de atributos do solo pela calagem superficial e incorporada a partir de pastagem natural. Rev Bras Ciência do Solo 24:797–805

Soil Survey Staff (2013) Simplified guide to soil taxonomy. USDA-Natural Resources Conservation Service, National Soil Survey Center, Lincoln

Un A, Sahin Y (2012) Determination of mass attenuation coefficients, effective atomic numbers, effective electron numbers and kermas for earth and Martian soils. Nucl Instrum Methods Phys Res Sect B Beam Interact Mater Atoms 288:42–47

van Raij B, Andrade JC de A, Cantarella H, Quaggio JA (2001) Análise química para avaliação da fertilidade de solos tropicais. Instituto Agronômico de Campinas, Campinas